ELSEVIER

Contents lists available at ScienceDirect

LITHOS

journal homepage: www.elsevier.com/locate/lithos





Sluggish rise of the western Gangdese mountains after India-Eurasia collision

Xuanyu Liu^{a,*}, Ming Tang^a, Wenrong Cao^b, Wei-Qiang Ji^c, Hao Chen^a

- ^a School of Earth and Space Sciences, Peking University, Beijing 100871, China
- ^b Department of Geological Sciences and Engineering, University of Nevada, Reno, NV 89557, United States of America
- c State Key Laboratory of Lithospheric Evolution, Institute of Geology and Geophysics, Chinese Academy of Sciences, P.O. Box 9825, Beijing 100029, China

ARTICLE INFO

Keywords: Tibetan geology Zircon Crustal thickness Eu anomaly Asian climate

ABSTRACT

With the most prominent topography on Earth, the Tibetan Plateau has profound influences on the hydrologic cycle and climate dynamics in Asia. However, the regional uplift history of the Tibetan Plateau remains highly debated. Here, we use europium anomalies and LREE/HREE ratio in detrital zircon, combined with whole-rock La/Yb_N ratio, to constrain the crustal thickness and topographic evolution of the Gangdese mountains in southern Tibet. Europium anomaly, controlled by pressure-sensitive minerals plagioclase and garnet, has been shown to correlate with crustal thickness. Our results reveal contrasting crustal thickening histories of the eastern (east of \sim 88°E) and western (west of \sim 88°E) parts of the Gangdese. Prior to the India-Eurasia collision (\sim 60–55 Ma), the crust of the eastern Gangdese thickened continuously from \sim 40 km to nearly 60 km, while the western Gangdese maintained a mildly thickened crust of $\sim \! 50$ km. Both parts underwent substantial thinning (to 40–45 km) immediately before the India-Eurasia collision, but the eastern Gangdese re-thickened rapidly afterwards. In the western Gangdese, post-collisional thickening was delayed until ~40-20 Ma, which resulted in a mild elevation of ~2000 m for most areas of southern Tibet until the late Oligocene. This diachronous uplift of the Gangdese after collision may have resulted from more mantle-derived magma additions in the eastern Gangdese before collision, which could rheologically weaken its lithosphere. We suggest that the diachronous uplift of the Gangdese after the India-Eurasia collision may have dominated the moisture transfer pattern across southern Tibet through the late Eocene and intensified the South Asian monsoon through the Oligocene-Miocene boundary (~25-20 Ma).

1. Introduction

The Tibetan Plateau, which has the world's thickest continental crust and highest elevation, was formed from the India-Eurasia continental collision, and profoundly affected the climate in Asia (Molnar and England, 1990). There are longstanding questions regarding the time at which the plateau attained its present crustal thickness and elevation, and whether or to what extent there are regional differences (Chung et al., 2005; Ding et al., 2022; Yin and Harrison, 2000). The Gangdese magmatic belt at the southern margin of the Tibetan Plateau lies immediately to the north of the Yarlung-Tsangpo suture zone (Fig. 1), where India initially collided with Eurasia at \sim 60–55 Ma (Ding et al., 2005; Hu et al., 2016; van Hinsbergen, 2022; Wu et al., 2014). Previous studies have attempted to reconstruct the crustal thickness of the Gangdese using various geochemical proxies, including whole-rock La/

 Yb_N ratio (N: chondrite normalized) (Sundell et al., 2021; Zhu et al., 2017), Nd and Hf isotope (DePaolo et al., 2019), and Eu/Eu* (chondrite normalized Eu/ $\sqrt{Sm \times Gd}$) in detrital zircon (Sundell et al., 2024; Tang et al., 2020a). But these studies mainly focused on the eastern Gangdese with only limited data for the more extensive western part. Further, even for the relatively well-studied eastern Gangdese, wholerock sample coverage is spatially and temporarily incomplete.

Magmatism in the Gangdese spans from \sim 240 Ma to \sim 10 Ma, displaying several magmatic flare-ups and lulls (Chapman and Kapp, 2017; Ma et al., 2022). The \sim 65–45 Ma flare-up formed a substantial part of the Gangdese Batholith and the massive Linzizong volcanic sequence (Fig. 1) (Ma et al., 2022). However, the Linzizong volcanics show contrasting distribution patterns, and they are more extensively exposed in the western Gangdese than in the eastern Gangdese (Fig. 1B). One possibility is that the Linzizong lavas have indeed erupted more

E-mail address: xuanyuliu@stu.pku.edu.cn (X. Liu).

^{*} Corresponding author.

intensely in the western Gangdese. Alternatively, Linzizong volcanics could be better preserved due to less surface uplifting and erosion in the western Gangdese over the last tens of million years (Fu et al., 2024). The latter scenario would be consistent with the eastward deepening of the exposure levels of the Gangdese crustal rocks from Lhasa to Nyingchi, evidenced by the increasing metamorphic grade and bedrock pressure toward the east (Cao et al., 2020).

Europium (Eu) anomaly or Eu/Eu* in zircon has been used to correlate with crustal thickness (Tang et al., 2020a). This correlation results from the combined effects of plagioclase and garnet fractionations, both of which are pressure-sensitive. In the thin crust corresponding with lower pressure, plagioclase crystallization depletes Eu²⁺ in the residual melt relative to Sm and Gd, because of the substitution of Eu^{2+} for Sr^{2+} (Ren, 2004). This effect leads to negative Eu anomaly (Eu/ Eu* < 1) in the melt, which is recorded by the subsequently crystallized zircon. As the crust thickens, intracrustal differentiation processes, through either anatexis or fractional crystallization, occur under elevated pressure conditions. Consequently, plagioclase crystallization is suppressed and thus reduces Eu depletion in the melt. Furthermore, garnet grows with crustal thickening, which preferentially incorporates Fe^{2+} , causing Fe^{3+}/Σ Fe in the melt to increase and therefore oxidizing Eu²⁺ to more compatible Eu³⁺. The net effect of both processes is to increase Eu/Eu* in zircon and make it possible to use detrital zircon measurements to reconstruct crustal thickness evolution (Tang et al., 2020a). Detrital zircon Eu/Eu* as a proxy for crustal thickness has been tested in eastern Gangdese, and the results are consistent with previously reported geologic records (Tang et al., 2020a; Zhu et al., 2017). On one hand, it is possible that magma crystallization and differentiation may occur throughout the crustal column from the source to the shallow magma chamber. So, the Eu/Eu* in zircon may reflect the integrated chemical evolution of magmas. However, as the crust thickens, the average/integrated depth of magmatic differentiation would increase systematically, leading to higher average Eu/Eu* in zircon. This also underscores the importance of sufficient analysis to derive robust results

on crustal thickness using the Eu/Eu*-in-zircon proxy (Tang et al., 2020a). On the other hand, magmatic oxygen fugacity may also affect Eu/Eu* in zircon, as indicated by recent simulations (Yakymchuk et al., 2023). However, oxygen fugacity of felsic magmas may also be controlled by the pressure of differentiation to a first order (Tang et al., 2018; Tang et al., 2020b). By contrast, the initial oxygen fugacity in the source region has little effect (Sun and Lee, 2022). Such a positive correlation between oxygen fugacity and crustal thickness has already been observed in the Gangdese belt (Tang et al., 2020b). For whole-rock La/ YbN and zircon LREE/HREE (light/heavy rare earth elements) proxies, they rely on similar pressure-sensitive minerals, including garnet, plagioclase, and/or amphibole. As the crust thickens, amphibole and garnet fractionate under higher pressure, depleting middle and heavy REEs (e.g., Yb), relative to LREEs (e.g., La), leading to elevated La/Yb_N (Profeta et al., 2015). Compared to the thickness proxies based on whole-rock samples, the Eu/Eu*-in-zircon proxy makes large-area sampling more effective and provides a higher temporal resolution record, particularly in regions where older igneous rocks are not preserved.

In this study, we combine Eu anomalies and LREE/HREE ratios of detrital zircon, together with available data on whole-rock La/Yb_N, to constrain the crustal thickening history of the eastern and western Gangdese magmatic belt since the Cretaceous. Our results reveal a significant difference in the pattern of crustal thickening between the eastern and western Gangdese, especially in ${\sim}60\text{--}40$ Ma, spanning the 20 Myr after India-Eurasia continental collision.

2. Brief geological background and samples

The Tibetan Plateau primarily consists of, from south to north: the Himalayas, Lhasa, Qiangtang, Songpan-Ganze, and Kunlun terranes (Kapp and DeCelles, 2019; Yin and Harrison, 2000). The Lhasa terrane is bounded by the Yarlung-Tsangpo suture zone in the south and the Bangong-Nujiang suture zone in the north and is subdivided into three

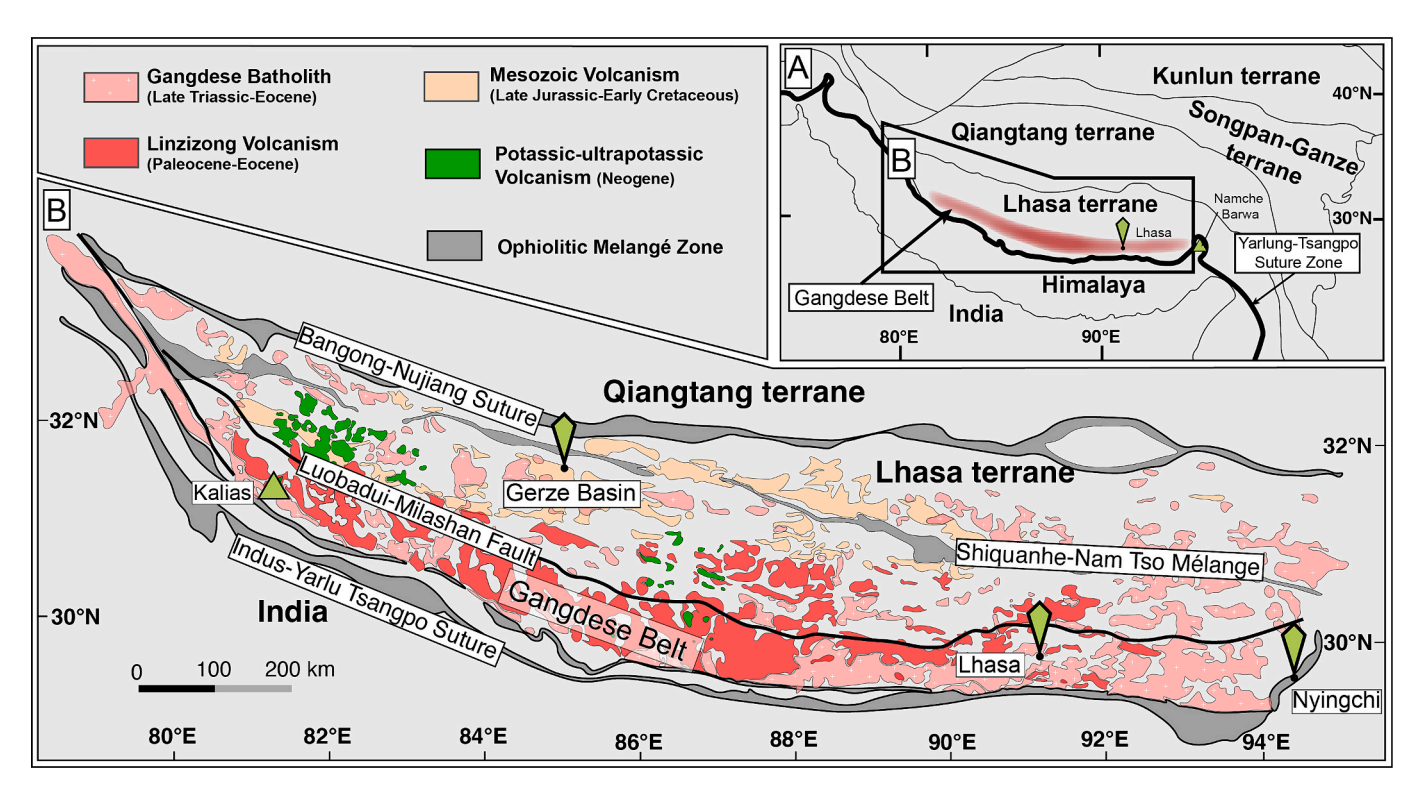


Fig. 1. Maps showing the Lhasa terrane's geological background.

(A) Simplified geological map of the entire Tibetan Plateau. Modified from Zhu et al. (2019). (B) Geological map of the Lhasa terrane showing the distribution of igneous rocks. Gangdese belt is predominantly distributed in the southern Lhasa terrane, south of the Luobadui-Milashan Fault. Modified from Hou et al. (2015).

subterranes: northern, southern, and central parts (Zhu et al., 2011). The Gangdese magmatic belt lies close to the southern margin of the Lhasa terrane, extending from Kailas (\sim 81°E) in the west to Namche Barwa (\sim 95°E) in the east (Fig. 1) (Ji et al., 2009; Yin and Harrison, 2000). This belt, now exhumed as the Gangdese Batholith, was formed from continental arc magmatism due to the northward subduction of the Tethyan Oceanic lithosphere beneath the Lhasa Terrane, and magmatism related to the continental collision between India and Asia (Zhu et al., 2019).

In this study, we focused on the Gangdese belt, which extends from $85^{\circ}E$ to $93^{\circ}E$, and adopted $\sim\!88~(\pm~0.5)~^{\circ}E$ as the boundary between the eastern and western Gangdese. This boundary marks the contrasting pattern of the Linzizong volcanic rocks which are substantially better preserved to the west of $\sim 88^{\circ}$ E (Fig. 1B). While our samples do not reach the far western Gangdese, the entire western Gangdese shows a consistent distribution pattern of Linzizong volcanics, suggesting similar erosion and thus uplift history in the area. We collected four modern river sand samples from the western Gangdese and one from the eastern Gangdese (Fig. 2). Similar to the sampling strategies of Tang et al. (2020a), we collected river sands from the tributaries that flow south through the Gangdese belt and merge into the main trunk of the Yarlu River. This sampling strategy avoids detrital zircon sourced from the Himalayas and restricts each sample to either eastern or western Gangdese (Fig. 2). The drainage area of samples from the eastern Gangdese spans from ~88.5°E to ~93.5°E, predominantly featuring intrusive rocks; the drainage area of samples from the western part extends from ~85.5°E to ~88.5°E, primarily characterized by volcanic rocks (Figs. 1 & 2). Detrital zircon grains were separated from the river sands for geochronology and trace element analysis through laser ablation-inductively coupled plasma-mass spectrometry (LA-ICP-MS). In addition, we incorporated the eastern Gangdese detrital zircon data (n = 1639 from 4 samples) from Tang et al. (2020a). In total, we obtained 2566 (5 samples) and 2039 (4 samples) analyses with U-Pb date and trace element concentration for detrital zircon of all ages for the eastern and western Gangdese, respectively. Data sets are provided in the Supplemental Material.

3. Materials and methods

3.1. Analytical methods and data filtering

We analyzed the in-situ U-Pb isotopes and trace elements of the detrital zircon grains by an ESI New Wave 193^{UC} (TwoVol2) laser ablation system coupled to an Agilent ICP-QQQ-MS 8900, at the Beijing Quick-Thermo Science & Technology Co., Ltd. The analysis was

conducted with a 30 μm spot size, $\sim 4~J/cm^2$ laser fluence, and a 5 Hz repetition rate. The aerosol was transported by high-purity He from the sample cell to the ICP. Before analysis, the ICP-QQQ-MS was tuned to keep a ThO/Th of <0.2%. Each analysis comprises 10 s background acquisition followed by 20 s data acquisition. The following isotopes were measured: ^{29}Si , ^{43}Ca , ^{45}Sc , ^{49}Ti , ^{89}Y , ^{91}Zr , ^{93}Nb , ^{139}La , ^{140}Ce , ^{141}Pr , ^{146}Nd , ^{147}Sm , ^{153}Eu , ^{157}Gd , ^{159}Tb , ^{163}Dy , ^{165}Ho , ^{166}Er , ^{169}Tm , ^{173}Yb , ^{175}Lu , ^{177}Hf , ^{181}Ta , ^{204}Pb , ^{206}Pb , ^{207}Pb , ^{208}Pb , ^{232}Th , and ^{238}U .

For U-Pb dating, we used zircon 91500 as the external standard and zircon GJ-1 as the monitor standard. Reference zircon GJ-1 has been demonstrated to have a homogeneous $^{206}\text{Pb}/^{238}\text{U}$ age of 610 ± 1.7 Ma by LA-ICP-MS (Elhlou et al., 2006). Our measurements of zircon GJ-1 have yielded a concordia age of 610.49 ± 0.68 Ma (Fig. S1). For trace elements, we used NIST 610 as the calibration standard and Si as the internal standard. Our results of zircon GJ-1 (Eu/Eu* = 0.81 \pm 0.11) are consistent with the value reported by Piazolo et al. (2017) (Fig. S1).

For the LREE/HREE ratio in zircon, we excluded Ce from the LREEs. Cerium has two valences, Ce³⁺ and Ce⁴⁺, with the latter preferentially incorporated into zircon (Shannon, 1976). The Ce⁴⁺/Ce³⁺ ratio is primarily controlled by oxygen fugacity and water contents (Smythe and Brenan, 2015). There is evidence suggesting that both factors are affected by crustal thickness. As the crust thickens, the magma becomes more oxidized (Tang et al., 2018; Tang et al., 2020b) and contains higher water contents (Klein et al., 2023). While oxidized magma contributes to Ce oxidation, leading to Ce⁴⁺ enrichment in the melt, elevated water content would suppress this oxidation (Smythe and Brenan, 2015). Due to the competing effect of water and oxygen fugacity, Ce concentrations in zircon and crustal thickness have a complex correlation. Notably, Ce concentrations in zircon are typically orders of magnitude higher than the other LREEs (La, Pr, Nd, Sm, and Eu) and dominate the LREE contents in zircon. Eu also has two valences (Eu²⁺ and Eu³⁺), but unlike Ce, water content and oxygen fugacity affect Eu/Eu* in the magma and zircon in the same way. Elevated water contents suppress plagioclase stabilization (Sisson and Grove, 1993), while a more oxidized magma composition results in higher proportions of Eu³⁺, which is more compatible than Eu²⁺ in zircon. Therefore, both processes contribute to increased Eu/Eu* in zircon as the crust thickens.

We excluded analyses with Th/U ratio of <0.1 to remove metamorphic zircon grains, which may have been affected by coeval growth of Th-rich minerals (e.g., monazite and allanite) during metamorphism (Rubatto, 2017). Additionally, we removed analysis with La >1 ppm, as they may have been compromised by inclusions, given that zircons typically have low LREE contents (Hoskin and Schaltegger, 2003). Zircon derived from S-type granites has consistently low Eu/Eu* and

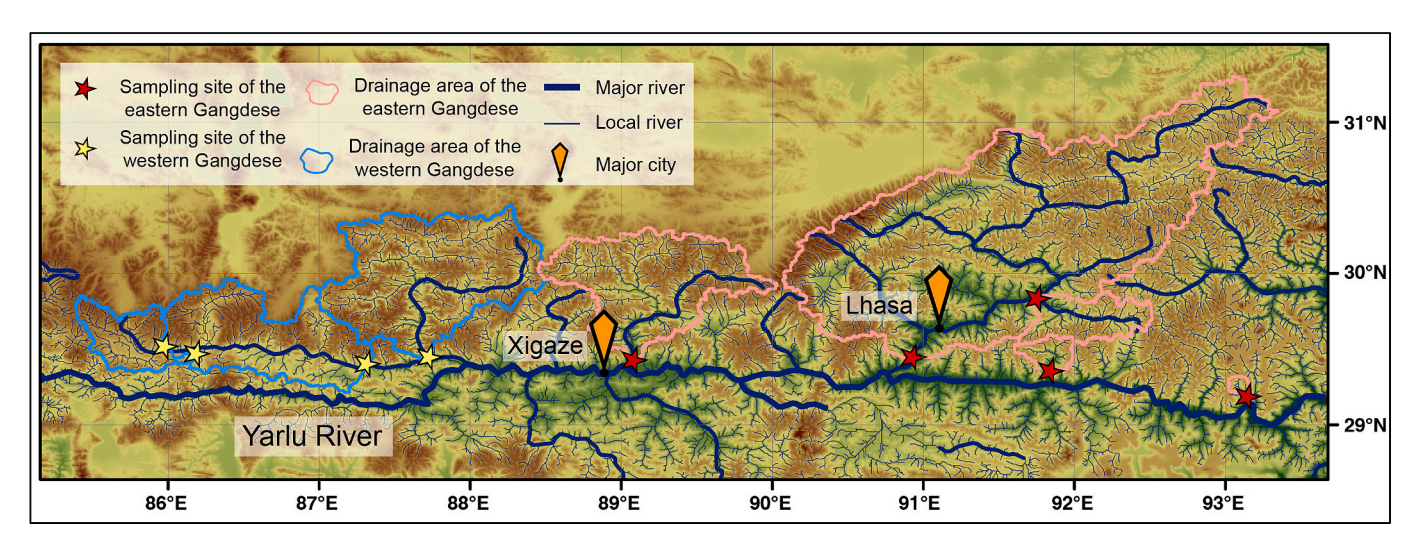


Fig. 2. Map showing the Yarlu River's tributaries, sampling sites, and drainage areas of each river sand sample. The four sand samples collected to the east of 90°E come from Tang et al. (2020a).

does not correlate with whole-rock La/Yb $_{\rm N}$ or crustal thickness (Tang et al., 2020a). This may be attributed to its Eu-depleted sedimentary protoliths (Rudnick and Gao, 2014) or high amounts of reduced phases like graphite that converts Eu $^{3+}$ to less-compatible Eu $^{2+}$ (Burnham and Berry, 2017). Based on the regional geological survey, the vast majority of the Gangdese batholith consists of I-type granites (Ji et al., 2009). Hence, we consider the influence of S-type granites to be negligible. When calculating the bin averages and errors, we excluded the analyses with the highest and lowest 10% Eu/Eu* in each 2 Myr bin to reduce scatter (Tang et al., 2020a). The screening processes would not change the crustal thickness evolution pattern (Fig. S2). After filtering, we were left with 1704 (the eastern Gangdese) and 1163 (the western Gangdese) sets of zircon data with both U-Pb age and trace element data within the 130–0 Ma range. All the results are provided in Dataset S1 as a separate file.

3.2. Calculation of the crustal thickness

We use detrital zircon Eu anomaly (chondrite normalized Eu/ $\sqrt{\text{Sm}} \times \text{Gd}$) proxy to calculate the crustal thickness (Tang et al., 2020a). Utilizing a dataset of 120 igneous samples with paired zircon-whole rock data over the world, and combining the whole-rock La/YbN relationship with crustal thickness and Eu/Eu* in zircon, Tang et al. (2020a) arrived

an empirical equation to calculate the crustal thickness:

$$H_{cal} = (84.2 \pm 9.2) \times Eu/Eu^*_{zircon} + (24.5 \pm 3.3)$$
 (1)

where H_{cal} represents the calculated crustal thickness (in km), while the uncertainties of the slope and intercept are two standard deviations. We have incorporated the uncertainties from the zircon Eu/Eu* proxy and the scatter within each bin into the calculation of crustal thickness.

3.3. Calculation of the paleo-elevation

We calculate the paleo-elevation assuming the Airy isostasy (Airy, 1855). In this model, all crustal blocks of the same density float above the denser asthenospheric mantle, and the pressure at the compensation depth is the sum of the pressure exerted by the overlying crust and mantle. Theoretically, the lithospheric mantle should also be considered in calculating the total buoyancy budget. However, given the minor density contrast between the lithospheric and asthenospheric mantle, as well as the presence of a relatively thin (similar to the crust) or even absent lithospheric mantle beneath the Lhasa terrane (Ji et al., 2014; Liang et al., 2018; Yue et al., 2012), we have ignored the influence of lithospheric mantle when calculating elevation. The paleo-elevation can be calculated by:

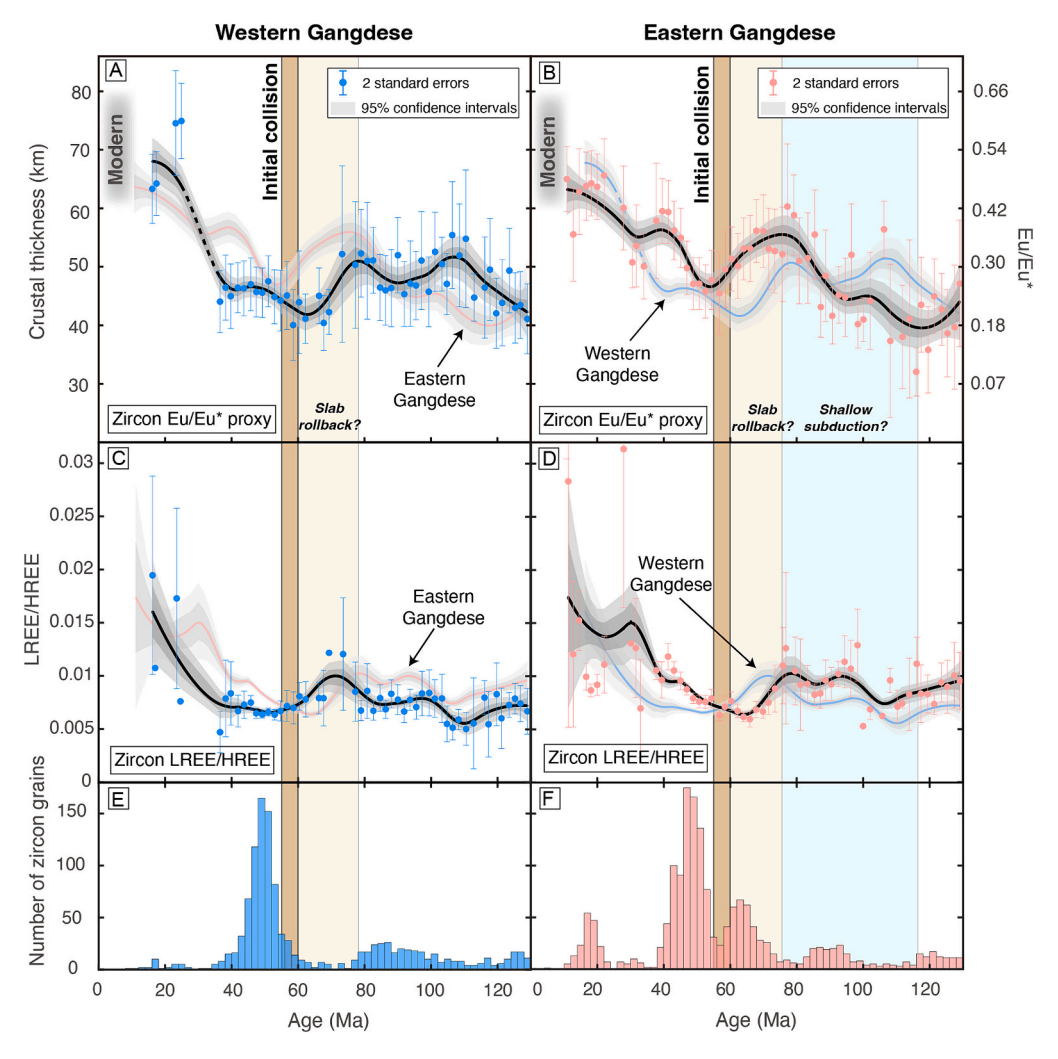


Fig. 3. Detrital zircon results and reconstructed crustal thickness for the eastern and western Gangdese, respectively. Data are plotted in each 2 m.y. bin with 2 standard errors. The black line in A-D indicates the fitted line. (A and B) Europium anomaly (right axis) and reconstructed crustal thickness (left axis) of the eastern Gangdese (n = 1704) and western Gangdese (n = 1704). The dashed line in the western Gangdese indicates insufficient data during that period. (C and D) The detrital zircon LREE/HREE ratio trend of the eastern and western Gangdese, respectively. (E and F) Age distribution of detrital zircon of the eastern and western Gangdese adopted in this study, respectively.

$$h = (H_{cal} - H_{ref}) \times \frac{\rho_m - \rho_c}{\rho_m}$$
 (2)

where h represents the calculated paleo-elevation. We assumed H_{ref} , which represents the reference crustal thickness, as \sim 35 km adopted from Molnar et al. (1993). The average continental crust density (ρ_c) is \sim 2.67 g/cm³ and the average mantle density (ρ_m) is \sim 3.27 g/cm³ (He et al., 2014).

4. Results

Zircon U-Pb dating results show that the eastern and western Gangdese have similar age patterns, with two main magmatic flare-ups in the Late Cretaceous and the early Eocene (Fig. 3E, F). Europium anomaly results show that, although the eastern and western Gangdese have similar present-day values, their changing patterns differ over the last 130 Myr (Fig. 3A, B). Our reconstructed patterns for both eastern and western Gangdese are mostly consistent with those of the detrital zircon LREE/HREE ratio and whole-rock La/Yb_N ratio (Figs. 3 & 4). However, there are some complexities associated with these two proxies. Low LREE contents in zircon make measurements challenging and the results are extremely sensitive to inclusion contamination, leading to a substantial scatter of data. The problem with whole-rock La/Yb_N approach is the paucity of samples, especially for the western Gangdese.

5. Discussion

According to the new analytical data, during most of the Late Cretaceous period (\sim 90–66 Ma), the western Gangdese crust was thinner than that of the continental crust in the eastern Gangdese. In the Late Cretaceous (\sim 110–80 Ma), the eastern Gangdese thickened from \sim 40 km to \sim 60 km (Fig. 3B), while the western Gangdese maintained a mildly thickened crust whose thickness fluctuated between \sim 40 and 50 km (Fig. 3A). Immediately before the India-Eurasia initial collision at \sim 60–55 Ma, both the western and eastern Gangdese crusts were thinned to 40–45 km (Fig. 3A, B). After the initial collision, the eastern Gangdese re-thickened within a few million years. However, in the western

Gangdese, crustal thickness remained between 40 and 45 km for another 20 Myr until the onset of post-collisional thickening at some time between 40 and 20 Ma (Fig. 3A).

5.1. Pre-collisional thickening pattern

The Late Cretaceous crustal thickening of the eastern Gangdese remains controversial (Ji et al., 2014; Tang et al., 2020a; Zhu et al., 2017). Both the whole-rock La/Yb_N ratio and zircon trace element data indicate crustal thickening (Figs. 3 & 4), yet some have attributed the highpressure signatures to the melting of subducted oceanic crusts (Zhu et al., 2017). We cannot entirely exclude the possible additions of slab melts, as our zircon proxy cannot directly distinguish these two origins. Nevertheless, the compression-induced thickening of the eastern Gangdese crust is more consistent with multiple lines of geological evidence, including N-directed crustal shortening, sedimentary transition from marine carbonate to fluvial sandstones in the Linzhou Basin, and tectonic burial of mid-lower crustal rocks (Cao et al., 2020; Kapp et al., 2007; Wang et al., 2020). By contrast, there is no direct geological evidence of crustal thickening of the western Gangdese. Previous studies have proposed a ridge subduction model during the Late Cretaceous (Zhang et al., 2010; Zhu et al., 2019), which could potentially account for the observed crustal thickening of the eastern Gangdese in this time period. But so far, this model may not fully explain the contrasting thickening patterns between the eastern and western Gangdese unless more details and further geological evidence are available, i.e., whether the ridge was parallel, perpendicular, or at an oblique angle with the trench. If the ridge was parallel to the trench along the Gangdese belt, the eastern and western Gangdese would share similar crustal thickening patterns and magmatic activities. In addition, if the ridge was subducted perpendicularly to the trench in the eastern Gangdese, this could potentially explain the crustal thickening of the eastern crust in the Late Cretaceous. However, this scenario introduces another issue—the timing of ridge subduction termination. Furthermore, if the ridge subduction was not perpendicular, then the western Gangdese crust would also thicken when the ridge subduction propagated to the west. The time lag for this thickening pattern along the Gangdese

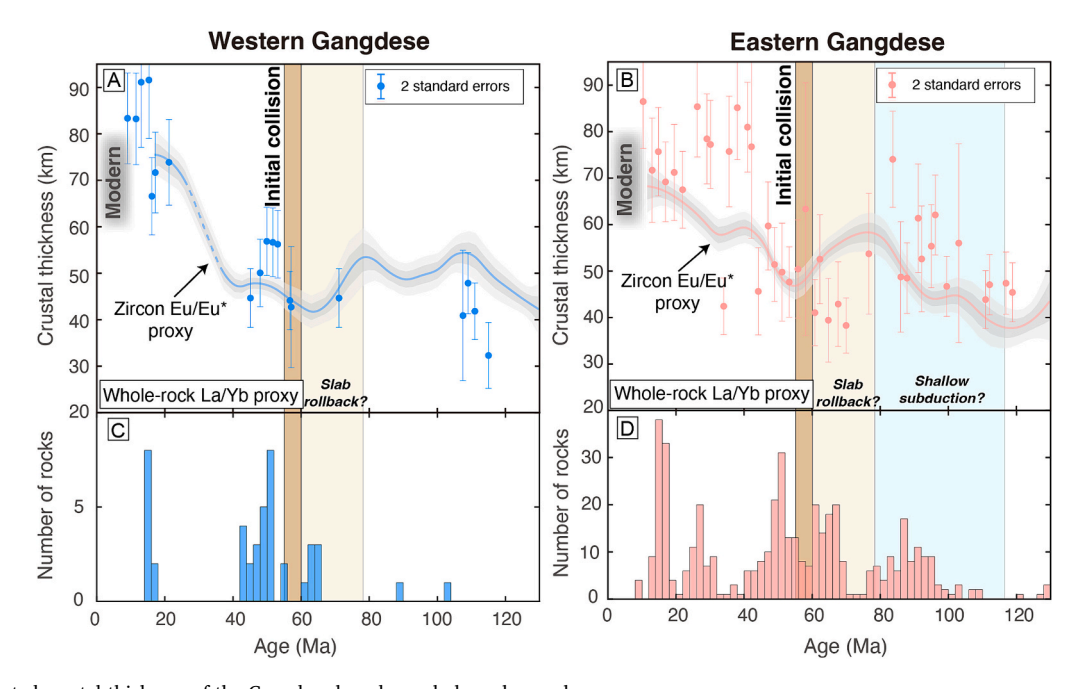


Fig. 4. Reconstructed crustal thickness of the Gangdese based on whole-rock samples. (A and B) The reconstructed crustal thickness of the eastern (n = 511) and western Gangdese (n = 170), respectively. Only limited whole-rock data is available for the western Gangdese. The data come from Chapman and Kapp (2017) and Zhu et al. (2017). (C and D) Age distribution of magmatic rocks of the eastern and western Gangdese, respectively. Compiled from Ji et al. (2014).

depends on the intersection angle between the ridge and the trench. Given so many uncertainties, the current ridge subduction model cannot provide a satisfactory explanation for our results.

Therefore, by applying a simple plate kinematic model, we propose that the different pre-collisional crustal thickening processes were driven by different degrees of tectonic shortening between the two parts of the Gangdese. In the Late Cretaceous, the oceanic slab subducting beneath the eastern Gangdese was younger according to global ocean basin reconstructions (Seton et al., 2012). Some argued for the existence of an additional ocean basin, such as the Xigaze back-arc ocean basin, between India and Asia during the Late Cretaceous (Kapp and DeCelles, 2019). However, the classic Greater India model appears to be supported by more geological evidence, including a recent comprehensive study incorporating palaeontologic, petrographic, and paleomagnetic data from the Sangdanlin section in southern Tibet (Meng et al., 2023). Given the limited relevant data in our research to thoroughly discuss this issue, we choose to accept the classic Greater India model that has been accepted by most of the community. Due to the more buoyant subducting slab, the convergence along the eastern Gangdese is characterized by a smaller subduction angle and lower subduction rate (Cross and Pilger Jr., 1982). Further, the Morondova mantle plume in the Late Cretaceous rotated the entire Indian Plate counterclockwise, causing an eastward increase of convergence rate along southern Tibet (van Hinsbergen et al., 2011). Kinematically, a high convergence rate coupled with a low subduction rate would inevitably lead to substantial upper plate shortening (Royden, 1993) and thus more efficient crustal thickening in the eastern Gangdese.

Predating the India-Eurasia continental collision is a \sim 15 Myr period (~75-60 Ma) of crustal thinning for both parts of the Gangdese. Delamination of dense arc roots (arclogites) has been widely invoked as an important mechanism in destroying thickened arc crust (Ducea et al., 2021). However, the delamination largely depends on the thickness of dense arc roots (Lee, 2014). It seems unlikely for delamination to take place synchronously along the entire Gangdese where the pre-thinning crustal thickness differed by $\sim \! 10$ km between the western and eastern segments (Fig. 3). We consider slab rollback as a more likely mechanism to account for this large-scale crustal thinning. The extension induced by slab rollback is supported by reinitiation and southward migration of arc magmatism at ~69 Ma (Chung et al., 2005; Zhu et al., 2019). Previous studies suggested a slab rollback event in the Late Cretaceous (90-70 Ma), supported by reconstructed crustal thickening history based on whole-rock La/Yb_N proxy (Kapp and DeCelles, 2019; Sundell et al., 2021). However, their time period shows a slight difference compared to ours. Given the lower temporal resolution of rock samples, which is also reflected in our whole-rock La/YbN data (Fig. 4), we believe our Eu/Eu* results might be more reliable.

5.2. Post-collisional thickening pattern

A more intriguing observation pertains to the contrasting crustal thickening histories of the eastern and western Gangdese after the initial India-Eurasia collision (Fig. 3). The eastern Gangdese thickened rapidly in response to the continental collision (~60-55 Ma), while the thickening in the western Gangdese was delayed by at least 20 Myr and initiated sometime between 40 and 20 Ma (Fig. 3). One possibility to account for these contrasting thickening patterns is related to diachronous collision along the Gangdese with the collision taking place earlier in the east. Earlier studies suggested that the Indian plate first collided with the Eurasia continent in the western Himalaya at ~55 Ma and closed eastwards (Beck et al., 1995; Rowley, 1996). Alternatively, Ding et al. (2017) proposed the initial collision first took place in the central Himalaya at $\sim\!65$ Ma and then closed both eastwards and westwards at \sim 55 Ma. However, none of these diachronous collision models can explain why the eastern Gangdese started to thicken 20 Myr earlier than the western Gangdese after the initial collision (Fig. 3). In fact, Hu et al. (2016) found that the Paleocene-Eocene sedimentary

successions of the western and central-eastern Himalaya can be correlated, and suggested that no evident time lag exists along the Himalaya during the initial collision at \sim 59 Ma. Therefore, diachronous collision is unlikely to have caused the contrasting thickening histories between the eastern and western Gangdese.

Alternatively, the contrasting post-collisional thickening patterns may reflect the distinct nature of the lithospheres beneath the western and eastern Gangdese prior to the collision. Evidence supporting this hypothesis comes from Hf isotopes probing the Gangdese deep crust. The eastern and western Gangdese exhibit differences in the Hf isotope compositions ($\epsilon_{Hf}(t)$) of the pre-collisional crust of the Lhasa terrane across ~88°E longitude (Hou et al., 2015). The eastern Gangdese has positive $\varepsilon_{Hf}(t)$ values (~ +3 to +15), indicating a juvenile crustal block; whereas the western Gangdese, similar to that of the central Lhasa terrane, is characterized by negative $\varepsilon_{Hf}(t)$ values (~ -14 to -1) (Fig. 5). This divide in crustal Hf isotopic compositions suggests that mantle magma addition to the crust was pervasive in the eastern Gangdese but limited in the western Gangdese before the continental collision. Such contrasting mantle magma addition may reflect the different alongstrike plate subduction processes along the Gangdese during Neo-Tethyan plate subduction, which may be related to the different ages of the subducting slabs (Seton et al., 2012) and convergence rates between the eastern and western Gangdese in the Late Cretaceous. A faster convergence in the eastern Gangdese may have been caused by Morondova mantle plume rotating the whole Indian Plate counterclockwise (van Hinsbergen et al., 2011).

Extensive mantle magma addition may have significantly changed the rheological structure of the eastern Gangdese lithosphere prior to the India-Eurasia collision. Juvenile melts extracted from the convecting mantle initially propagate through diffuse porous flow, heating and reacting with the overlying lithosphere which leads to strength reduction. Petrological experiments suggest that a small amount of melt (~7%) could significantly reduce the lithospheric strength (Hirth and Kohlstedt, 1995; Rosenberg and Handy, 2005). Numerical modeling results also indicate that mantle-derived magma can weaken the lithosphere and cause lithosphere-scale deformation during subduction and continental collision (Gerya and Meilick, 2011; Kelly et al., 2019; Zhang et al., 2022). Therefore, the massive juvenile magma addition in the subduction phase not only altered the crustal composition of the eastern Gangdese but also rheologically weakened its lithosphere. This rheological weakening may have led to a high lithospheric strain rate and immediate thickening after the collision.

5.3. Diachronous uplift of the Gangdese mountains

The contrasting thickening histories between the eastern and western Gangdese would cause diachronous uplift processes of southern Tibet (Fig. 6A, B). Using our reconstructed crustal thickness results and Airy isostasy, we calculated the paleo-elevation for the western and eastern Gangdese (Fig. 6A, B). We find that the eastern Gangdese rose immediately after the collision and attained an elevation of ~4000 m at ~40 Ma, while the western Gangdese may have remained at ~2000 m until the late Oligocene (Fig. 6A, B). The western Gangdese accounts for more than half of southern Tibet along strike. This means that the majority part of southern Tibet may have not risen to its present-day elevation of >4000 m until the late Oligocene. Since steeper topography could lead to a higher denudation rate (Larsen et al., 2014), the diachronous uplift of the Gangdese would also lead to stronger denudation of the eastern Gangdese, which would explain the preservation bias of the Linzizong volcanics between the eastern and western Gangdese.

The diachronous uplift seems to have existed not only in the Gangdese mountains but also in the inland areas to the north. Several paleo-altimetry studies reveal a relatively high topography (>3000 m) in southeastern Tibet at \sim 40 Ma, including the Relu (\sim 29°N, 101°E), Nangqian (\sim 32°N, 96.5°E) and Gonjo basin (\sim 31°N, 97°E) (He et al.,

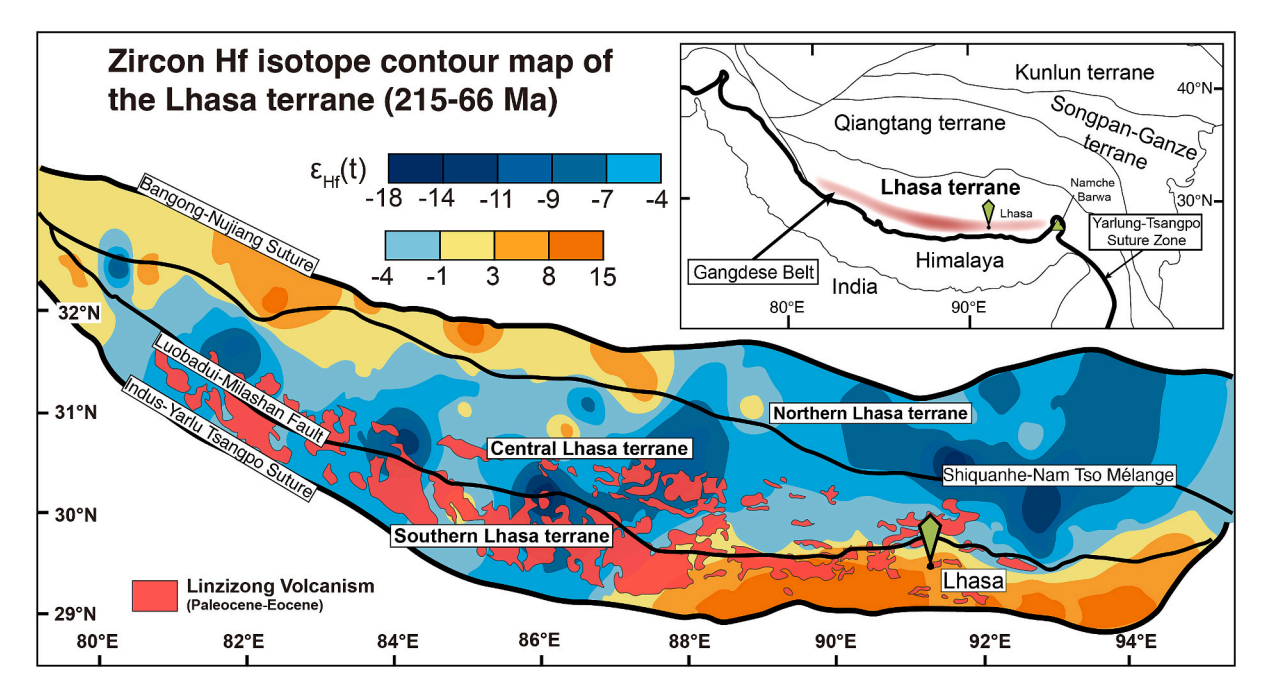


Fig. 5. Zircon Hf isotope contour map of the granitoid rocks and felsic volcanics in the Lhasa terrane from 215 to 66 Ma. The area highlighted in dark red refers to the Linzizong volcanism, which roughly corresponds to the areas exhibiting negative $\varepsilon_{Hf}(t)$ values. This contour map was based on 4762 sets of zircon Lu-Hf and U-Pb isotope analysis and produced in ArcGIS using the inverse distance weighted interpolation method (Hou et al., 2015). Modified from Hou et al. (2015). (For interpretation of the references to colour in this figure legend, the reader is referred to the web version of this article.)

2022; Li et al., 2018; Xiong et al., 2020). On the contrary, the elevation of central Tibet, including the Lunpola basin (\sim 32°N, 89°E), was generally low (<2000 m) at \sim 38 Ma and rose to >4000 m by 29 Ma (Fang et al., 2020; Xiong et al., 2022). The Nima basin (\sim 31.5°N, 87°E), located farther west, may have maintained a low elevation and subtropical environment until the late Oligocene (\sim 26 Ma) (DeCelles et al., 2007; Deng and Jia, 2018). This diachronous uplift scenario, where eastern Tibet rose earlier than the western part, is consistent with that of the Gangdese mountains.

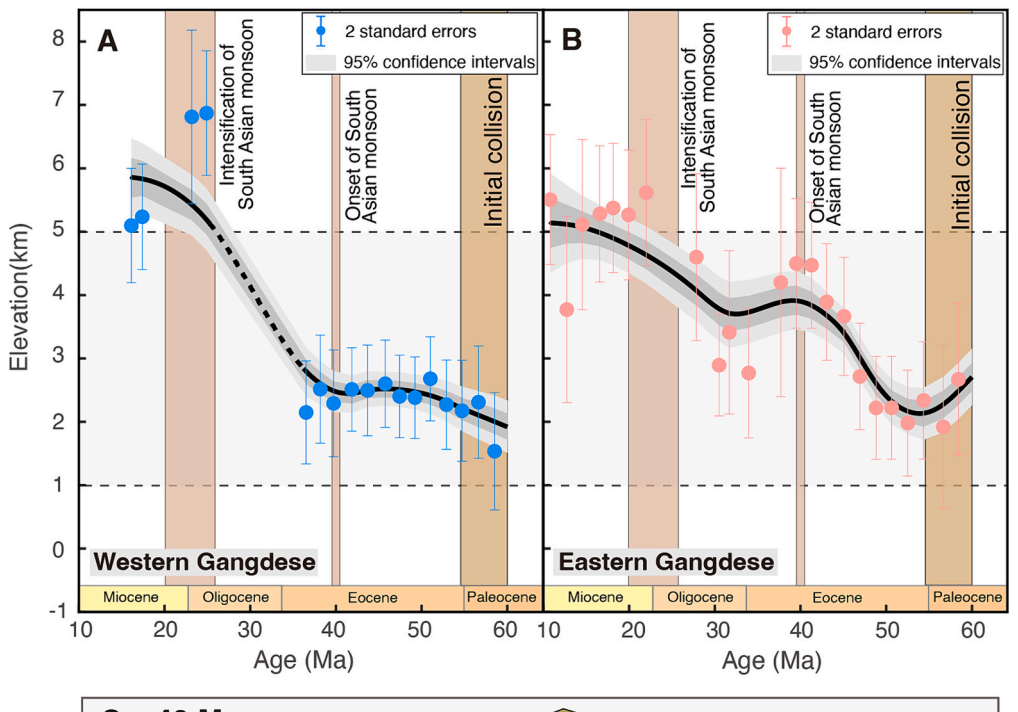
6. Paleoclimate implications

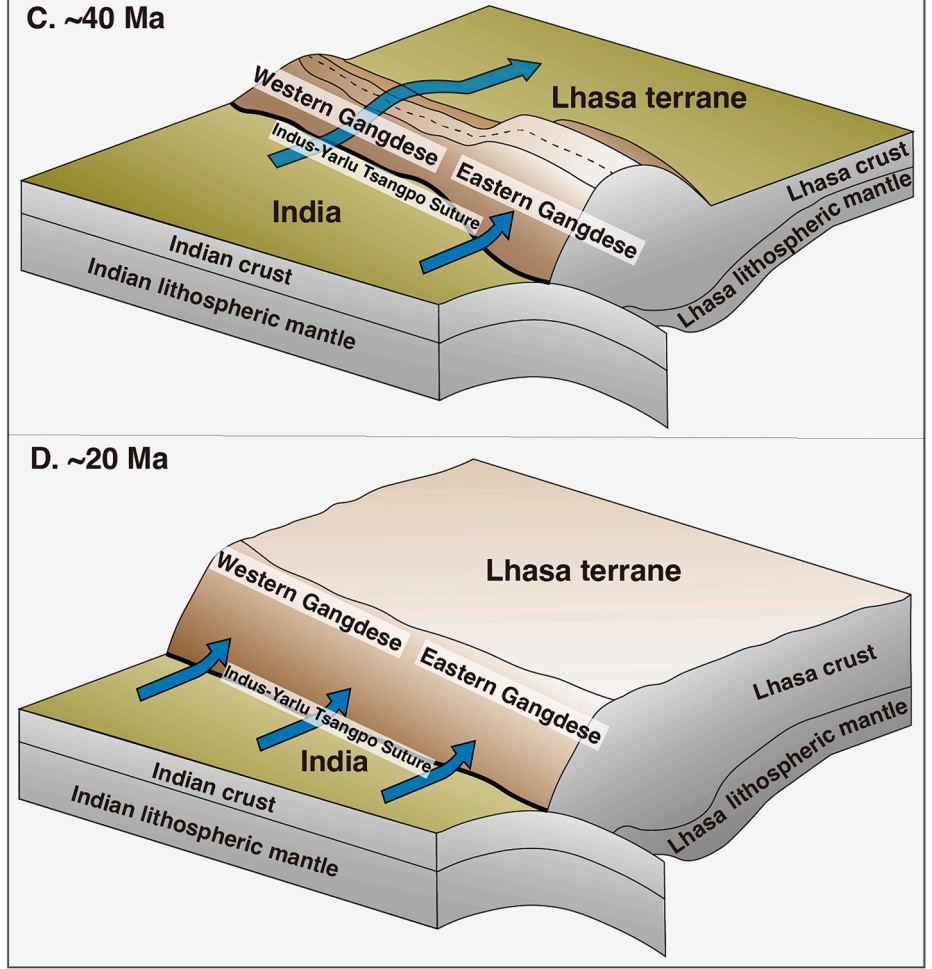
The diachronous uplift of the Gangdese mountains bears important implications for the evolution of regional paleoclimate and Asian monsoon systems. Recent studies of the basins in the Central Tibetan Valley, located on the north of the Gangdese, suggested that the Central Tibetan Valley was at moderate elevation of ~2000 m in the late Eocene with a humid subtropical climate (Su et al., 2020). Such subtropical climate in central Tibet requires a continued inflow of moisture. Although the moisture could be sourced from Westerlies and monsoons from the southeast (Xiong et al., 2022), the efficiency of such longdistance transport is uncertain. By contrast, if the western Gangdese was low in the late Eocene, as our data suggest, moisture from the south could pass over the western Gangdese and be transported to the Central Tibetan Valley directly (Fig. 6C). In addition, Wei et al. (2016) discovered a type of foraminifera (Lagena laevis) associated with lagoon and estuarine environments in the upper Eocene strata of the Gerze basin (Fig. 1B) in the western Central Tibetan Valley. Most researchers, including Wei et al. (2016), believed that Lagena laevis was transported by extreme storms from the Pamir Sea in the west, because the passageways from the Himalayan Sea in the south were thought to be blocked by the high-elevation Gangdese mountains in the late Eocene (Ding et al., 2014; Zhu et al., 2017). Our results of a low-elevation western Gangdese mountain during the entire Eocene make the Himalayan Sea a more likely source of the foraminifera, given that the Gerze Basin is much closer to the Himalayan Sea in the south (~200 km) than to the Pamir Sea in the west (\sim 500 km).

A low-elevation western Gangdese in the Eocene and possibly the Oligocene would also change our understanding of the evolution of the South Asian Monsoon. The rise of the southern Tibetan Plateau, mainly comprising the Gangdese and Himalayan mountains, is believed to have been responsible for the formation of the South Asian Monsoon, which had a profound impact on the climate in the Indian subcontinent (Boos and Kuang, 2010; Jin et al., 2023; Wu et al., 2022). Recent studies suggest that the monsoon may have been present in the late Eocene (Licht et al., 2014) and undergone significant intensification at 25-20 Ma (Clift and Webb, 2019). The Himalayan Mountains were only \sim 2000 m at 25–20 Ma, then rose rapidly, reaching \sim 4000 m at 19–18 Ma (Ding et al., 2022; Gébelin et al., 2013; Xu et al., 2018). While the Himalayas may have contributed to the Asian monsoon system, the Gangdese mountains, which have received less attention in the past, rose earlier and coincided with the intensification of the South Asian monsoon. We suggest that this intensification may be linked to the uplift of the western Gangdese mountains near the Oligocene-Miocene boundary (at ~25-20 Ma), which blocked the northward transport of moisture and enhanced the precipitation in South Asia (Fig. 6C, D).

7. Conclusion

Our results based on Eu anomalies and LREE/HREE ratios of detrital zircon and whole-rock La/Yb_N ratios reveal a contrasting crustal thickening pattern between the eastern and western Gangdese, particularly in the 20 Myr after India-Eurasia continental collision ($\sim\!60\text{--}55$ Ma). Before the collision, the entire Gangdese crust was thinned to 40–45 km. Immediately after that, the eastern Gangdese crust re-thickened rapidly, whereas the western part remained thin at least in $\sim\!60\text{--}40$ Ma and started to thicken at sometime between $\sim\!40\text{--}20$ Ma. The delayed post-collisional crustal thickening in the western Gangdese may have resulted in a relatively lower elevation ($\sim\!2000$ m) in the western Gangdese at least in the Eocene. The sluggish rise of the western Gangdese may be related to less lithospheric weakening by mantle addition than in the eastern Gangdese. The diachronous uplift likely played a key role in maintaining the humid subtropical climate in the Central Tibetan Valley through the late Eocene and intensifying the South Asian monsoon





(caption on next page)

Fig. 6. Diachronous uplift of the Gangdese mountains.

(A and B) Calculated elevation of the eastern and western Gangdese, respectively. The eastern Gangdese started to uplift immediately after the initial collision, while the western Gangdese was delayed by at least \sim 20 Myr to start uplifting. (C) At \sim 40 Ma, the eastern Gangdese attained an elevation of \sim 4000 m, whereas the western Gangdese remained at a relatively low elevation of \sim 2000 m. The moisture from the south could pass over the low western Gangdese mountains and enter the Central Tibetan Valley. (D) At \sim 20 Ma, the whole Gangdese uplifted as great mountains with an average elevation of \sim 5000 m, blocking the northward transport of moisture.

through the Oligocene-Miocene boundary (at \sim 25–20 Ma).

CRediT authorship contribution statement

Xuanyu Liu: Conceptualization, Formal analysis, Investigation, Visualization, Writing – original draft, Writing – review & editing, Data curation. **Ming Tang:** Conceptualization, Funding acquisition, Investigation, Writing – review & editing, Data curation. **Wenrong Cao:** Funding acquisition, Writing – review & editing, Investigation. **Wei-Qiang Ji:** Investigation, Writing – review & editing. **Hao Chen:** Data curation, Investigation, Writing – review & editing.

Acknowledgments

This work was supported by the National Natural Science Foundation of China (grants 41888101, 42125302, 42073026, and 91755000). W. Cao is grateful for the support from NSF-2221618. M. Tang is benefited from the support of the Xplorer Prize. We thank two anonymous reviewers for their constructive comments and editor Rui Wang for efficient handling. We are grateful for the discussion with Dr. Zi-Hua Tang, and Dr. Zhi-Yong Zhang's assistance in the LA-ICP-MS analysis.

Appendix A. Supplementary data

Supplementary data to this article can be found online at https://doi. org/10.1016/j.lithos.2024.107640.

References

- Airy, G.B., 1855. On the computation of the effect of the attraction of Mountain-Masses, as disturbing the apparent astronomical latitude of stations in geodetic surveys. Philos. Trans. R. Soc. Lond. 145, 101–104.
- Beck, R.A., Burbank, D.W., Sercombe, W.J., Riley, G.W., Barndt, J.K., Berry, J.R., Afzal, J., Khan, A.M., Jurgen, H., Metje, J., Cheema, A., Shafique, N.A., Lawrence, R. D., Khan, M.A., 1995. Stratigraphic evidence for an early collision between Northwest India and Asia. Nature 373 (6509), 55–58.
- Boos, W.R., Kuang, Z., 2010. Dominant control of the south Asian monsoon by orographic insulation versus plateau heating. Nature 463 (7278), 218–222.
- Burnham, A.D., Berry, A.J., 2017. Formation of Hadean granites by melting of igneous crust. Nat. Geosci. 10 (6), 457–461.
- Cao, W., Yang, J., Zuza, A.V., Ji, W.-Q., Ma, X.-X., Chu, X., Burgess, Q.P., 2020. Crustal tilting and differential exhumation of Gangdese Batholith in southern Tibet revealed by bedrock pressures. Earth Planet. Sci. Lett. 543, 116347.
- Chapman, J.B., Kapp, P., 2017. Tibetan magmatism database. Geochem. Geophys. Geosyst. 18 (11), 4229–4234.
- Chung, S.-L., Chu, M.-F., Zhang, Y., Xie, Y., Lo, C.-H., Lee, T.-Y., Lan, C.-Y., Li, X., Zhang, Q., Wang, Y., 2005. Tibetan tectonic evolution inferred from spatial and temporal variations in post-collisional magmatism. Earth Sci. Rev. 68 (3), 173–196.
- Clift, P.D., Webb, A.A.G., 2019. A History of the Asian Monsoon and its Interactions with Solid Earth Tectonics in Cenozoic South Asia: Geological Society, London, Special Publications, 483, p. 631 no. 1.
- Cross, T.A., Pilger Jr., R.H., 1982. Controls of subduction geometry, location of magmatic arcs, and tectonics of arc and back-arc regions. GSA Bull. 93 (6), 545–562.
- DeCelles, P.G., Quade, J., Kapp, P., Fan, M., Dettman, D.L., Ding, L., 2007. High and dry in Central Tibet during the late Oligocene. Earth Planet. Sci. Lett. 253 (3), 389–401.
- Deng, L., Jia, G., 2018. High-relief topography of the Nima basin in central Tibetan
 Plateau during the mid-Cenozoic time. Chem. Geol. 493, 199–209.
 DePaolo, D.J., Harrison, T.M., Wielicki, M., Zhao, Z., Zhu, D.-C., Zhang, H., Mo, X., 2019.
- DePaolo, D.J., Harrison, T.M., Wielicki, M., Zhao, Z., Zhu, D.-C., Zhang, H., Mo, X., 2019. Geochemical evidence for thin syn-collision crust and major crustal thickening between 45 and 32 Ma at the southern margin of Tibet. Gondwana Res. 73, 123–135.
- Ding, L., Kapp, P., Wan, X., 2005. Paleocene–Eocene record of ophiolite obduction and initial India-Asia collision, south central Tibet. Tectonics 24 (3).
- Ding, L., Xu, Q., Yue, Y., Wang, H., Cai, F., Li, S., 2014. The Andean-type Gangdese Mountains: Paleoelevation record from the Paleocene–Eocene Linzhou Basin. Earth Planet. Sci. Lett. 392, 250–264.
- Ding, L., Maksatbek, S., Cai, F., Wang, H., Song, P., Ji, W., Xu, Q., Zhang, L., Muhammad, Q., Upendra, B., 2017. Processes of initial collision and suturing between India and Asia. Sci. China Earth Sci. 60 (4), 635–651.

- Ding, L., Kapp, P., Cai, F., Garzione, C.N., Xiong, Z., Wang, H., Wang, C., 2022. Timing and mechanisms of Tibetan Plateau uplift. Nat. Rev. Earth Environ. 3 (10), 652–667.
- Ducea, M.N., Chapman, A.D., Bowman, E., Balica, C., 2021. Arclogites and their role in continental evolution; part 2: Relationship to batholiths and volcanoes, density and foundering, remelting and long-term storage in the mantle. Earth Sci. Rev. 214, 103476
- Elhlou, S., Belousova, E., Griffin, W.L., Pearson, N.J., O'Reilly, S.Y., 2006. Trace element and isotopic composition of GJ-red zircon standard by laser ablation. Geochim. Cosmochim. Acta 70 (18) (p. 158–158).
- Fang, X., Dupont-Nivet, G., Wang, C., Song, C., Meng, Q., Zhang, W., Nie, J., Zhang, T., Mao, Z., Chen, Y., 2020. Revised chronology of Central Tibet uplift (Lunpola Basin). Sci. Adv. 6 (50) (eaba7298).
- Fu, H., Kereszturi, G., Cheng, Q., Wang, R., Smith, A.G.G., 2024. Deciphering differential exhumation in the Gangdese orogen in southern Tibet using exposed porphyry alteration systems and geomorphic analysis. GSA Bull. https://doi.org/10.1130/ B37086.1.
- Gébelin, A., Mulch, A., Teyssier, C., Jessup, M.J., Law, R.D., Brunel, M., 2013. The miocene elevation of Mount Everest. Geology 41 (7), 799–802.
- Gerya, T.V., Meilick, F.I., 2011. Geodynamic regimes of subduction under an active margin: effects of rheological weakening by fluids and melts. J. Metamorph. Geol. 29 (1) 7–31
- He, R., Liu, G., Golos, E., Gao, R., Zheng, H., 2014. Isostatic gravity anomaly, lithospheric scale density structure of the northern Tibetan plateau and geodynamic causes for potassic lava eruption in Neogene. Tectonophysics 628, 218–227.
- He, S., Ding, L., Xiong, Z., Spicer, R.A., Farnsworth, A., Valdes, P.J., Wang, C., Cai, F., Wang, H., Sun, Y., Zeng, D., Xie, J., Yue, Y., Zhao, C., Song, P., Wu, C., 2022. A distinctive Eocene Asian monsoon and modern biodiversity resulted from the rise of eastern Tibet. Sci. Bull. 67 (21), 2245–2258.
- Hirth, G., Kohlstedt, D.L., 1995. Experimental constraints on the dynamics of the partially molten upper mantle: Deformation in the diffusion creep regime. J. Geophys. Res. Solid Earth 100 (B2), 1981–2001.
- Hoskin, P.W.O., Schaltegger, U., 2003. The composition of zircon and igneous and metamorphic petrogenesis. Rev. Mineral. Geochem. 53 (1), 27–62.
- Hou, Z., Duan, L., Lu, Y., Zheng, Y., Zhu, D., Yang, Z., Yang, Z., Wang, B., Pei, Y., Zhao, Z., McCuaig, T.C., 2015. Lithospheric architecture of the Lhasa Terrane and its Control on ore deposits in the Himalayan-Tibetan orogen*. Econ. Geol. 110 (6), 1541–1575.
- Hu, X., Garzanti, E., Wang, J., Huang, W., An, W., Webb, A., 2016. The timing of India-Asia collision onset – Facts, theories, controversies. Earth Sci. Rev. 160, 264–299
- Ji, W.-Q., Wu, F.-Y., Chung, S.-L., Li, J.-X., Liu, C.-Z., 2009. Zircon U–Pb geochronology and Hf isotopic constraints on petrogenesis of the Gangdese batholith, southern Tibet. Chem. Geol. 262 (3), 229–245.
- Ji, W.-Q., Wu, F.-Y., Chung, S.-L., Liu, C.-Z., 2014. The Gangdese magmatic constraints on a latest cretaceous lithospheric delamination of the Lhasa terrane, southern Tibet. Lithos 210-211, 168–180.
- Jin, C.-S., Xu, D., Li, M., Hu, P., Jiang, Z., Liu, J., Miao, Y., Wu, F., Liang, W., Zhang, Q., Su, B., Liu, Q., Zhang, R., Sun, J., 2023. Tectonic and orbital forcing of the south Asian monsoon in Central Tibet during the late Oligocene. Proc. Natl. Acad. Sci. 120 (15), e2214558120.
- Kapp, P., DeCelles, P.G., 2019. Mesozoic–Cenozoic geological evolution of the Himalayan-Tibetan orogen and working tectonic hypotheses. Am. J. Sci. 319 (3), 159.
- Kapp, P., DeCelles, P.G., Gehrels, G.E., Heizler, M., Ding, L., 2007. Geological records of the Lhasa-Qiangtang and Indo-Asian collisions in the Nima area of Central Tibet. GSA Bull. 119 (7–8), 917–933.
- Kelly, S., Beaumont, C., Butler, J.P., 2019. Inherited terrane properties explain enigmatic post-collisional Himalayan-Tibetan evolution. Geology 48 (1), 8–14.
- Klein, B.Z., Jagoutz, O., Schmidt, M.W., Kueter, N., 2023. A global assessment of the controls on the fractionation of arc magmas. Geochem. Geophys. Geosyst. 24 (5) (e2023GC010888).
- Larsen, I.J., Montgomery, D.R., Greenberg, H.M., 2014. The contribution of mountains to global denudation. Geology 42 (6), 527–530.
- Lee, C.T.A., 2014. 4.12 Physics and chemistry of deep continental crust recycling. In: Holland, H.D., Turekian, K.K. (Eds.), Treatise on Geochemistry, Second ed. Oxford, Elsevier, pp. 423–456.
- Li, L., Fan, M., Davila, N., Jesmok, G., Mitsunaga, B., Tripati, A., Orme, D., 2018. Carbonate stable and clumped isotopic evidence for late Eocene moderate to high elevation of the east-central Tibetan Plateau and its geodynamic implications. GSA Bull. 131 (5–6), 831–844.
- Liang, H., Jin, S., Wei, W., Gao, R., Ye, G., Zhang, L., Yin, Y., Lu, Z., 2018. Lithospheric electrical structure of the middle Lhasa terrane in the south Tibetan plateau. Tectonophysics 731-732, 95–103.
- Licht, A., van Cappelle, M., Abels, H.A., Ladant, J.B., Trabucho-Alexandre, J., France-Lanord, C., Donnadieu, Y., Vandenberghe, J., Rigaudier, T., Lécuyer, C., Terry Jr., D., Adriaens, R., Boura, A., Guo, Z., Soe, A.N., Quade, J., Dupont-Nivet, G., Jaeger, J.J., 2014. Asian monsoons in a late Eocene greenhouse world. Nature 513 (7519), 501–506.

- Ma, X., Attia, S., Cawood, T., Cao, W., Xu, Z., Li, H., 2022. Arc tempos of the Gangdese batholith, southern Tibet. J. Geodyn. 149, 101897.
- Meng, J., Gilder, S.A., Tan, X., Li, X., Li, Y., Luo, H., Suzuki, N., Wang, Z., Chi, Y., Zhang, C., Wang, C., 2023. Strengthening the argument for a large Greater India. Proc. Natl. Acad. Sci. 120 (33), e2305928120.
- Molnar, P., England, P., 1990. Late Cenozoic uplift of mountain ranges and global climate change: chicken or egg? Nature 346 (6279), 29–34.
- Molnar, P., England, P., Martinod, J., 1993. Mantle dynamics, uplift of the Tibetan Plateau, and the Indian Monsoon. Rev. Geophys. 31 (4), 357–396.
- Piazolo, S., Belousova, E., La Fontaine, A., Corcoran, C., Cairney, J.M., 2017. Trace element homogeneity from micron- to atomic scale: Implication for the suitability of the zircon GJ-1 as a trace element reference material. Chem. Geol. 456, 10–18.
- Profeta, L., Ducea, M.N., Chapman, J.B., Paterson, S.R., Gonzales, S.M.H., Kirsch, M., Petrescu, L., DeCelles, P.G., 2015. Quantifying crustal thickness over time in magmatic arcs. Sci. Rep. 5 (1), 17786.
- Ren, M., 2004. Partitioning of Sr, Ba, Rb, Y, and LREE between alkali feldspar and peraluminous silicic magma. Am. Mineral. 89 (8–9), 1290–1303.
- Rosenberg, C.L., Handy, M.R., 2005. Experimental deformation of partially melted granite revisited: implications for the continental crust. J. Metamorph. Geol. 23 (1), 19278
- Rowley, D.B., 1996. Age of initiation of collision between India and Asia: a review of stratigraphic data. Earth Planet. Sci. Lett. 145 (1), 1–13.
- Royden, L.H., 1993. The tectonic expression slab pull at continental convergent boundaries. Tectonics 12 (2), 303–325.
- Rubatto, D., 2017. Zircon: the metamorphic mineral. Rev. Mineral. Geochem. 83 (1), 261–295.
- Rudnick, R.L., Gao, S., 2014. 4.1 Composition of the continental crust. In: Holland, H. D., Turekian, K.K. (Eds.), Treatise on Geochemistry, Second ed. Oxford, Elsevier, pp. 1–51
- Seton, M., Müller, R.D., Zahirovic, S., Gaina, C., Torsvik, T., Shephard, G., Talsma, A., Gurnis, M., Turner, M., Maus, S., Chandler, M., 2012. Global continental and ocean basin reconstructions since 200Ma. Earth Sci. Rev. 113 (3), 212–270.
- Shannon, R.D., 1976. Revised effective ionic radii and systematic studies of interatomic distances in halides and chalcogenides. Acta Crystallogr. Sec. A 32 (5), 751–767.
- Sisson, T.W., Grove, T.L., 1993. Experimental investigations of the role of H2O in calcalkaline differentiation and subduction zone magmatism. Contrib. Mineral. Petrol. 113 (2), 143–166.
- Smythe, D.J., Brenan, J.M., 2015. Cerium oxidation state in silicate melts: combined fO2, temperature and compositional effects. Geochim. Cosmochim. Acta 170, 173–187.
- Su, T., Spicer, R.A., Wu, F.-X., Farnsworth, A., Huang, J., Rio, C.D., Deng, T., Ding, L., Deng, W.-Y.-D., Huang, Y.-J., Hughes, A., Jia, L.-B., Jin, J.-H., Li, S.-F., Liang, S.-Q., Liu, J., Liu, X.-Y., Sherlock, S., Spicer, T., Srivastava, G., Tang, H., Valdes, P., Wang, T.-X., Widdowson, M., Wu, M.-X., Xing, Y.-W., Xu, C.-L., Yang, J., Zhang, C., Zhang, S.-T., Zhang, X.-W., Zhao, F., Zhou, Z.-K., 2020. A Middle Eocene lowland humid subtropical "Shangri-La" ecosystem in central Tibet. Proc. Natl. Acad. Sci. 117 (52), 32989–32995.
- Sun, C., Lee, C.-T.A., 2022. Redox evolution of crystallizing magmas with C-H-O-S volatiles and its implications for atmospheric oxygenation. Geochim. Cosmochim. Acta 338, 302–321.
- Sundell, K.E., Laskowski, A.K., Howlett, C., Kapp, P., Ducea, M., Chapman, J.B., Ding, L., 2024. Episodic late cretaceous to Neogene crustal thickness variation in southern Tibet. Terra Nova 36, 45–52.
- Sundell, K.E., Laskowski, A.K., Kapp, P.A., Ducea, M.N., Chapman, J.B., 2021. Jurassic to Neogene quantitative crustal thickness estimates in southern Tibet. GSA Today 31 (6). 4–10.
- Tang, M., Erdman, M., Eldridge, G., Lee, C.-T.A., 2018. The redox "filter" beneath magmatic orogens and the formation of continental crust. Sci. Adv. 4 (5) (p. eaar4444)

- Tang, M., Ji, W.-Q., Chu, X., Wu, A., Chen, C., 2020a. Reconstructing crustal thickness evolution from europium anomalies in detrital zircons. Geology 49 (1), 76–80.
- Tang, M., Lee, C.-T.A., Ji, W.-Q., Wang, R., Costin, G., 2020b. Crustal thickening and endogenic oxidation of magmatic sulfur. Sci. Adv. 6 (31) (p. eaba6342).
- van Hinsbergen, D.J.J., 2022. Indian Plate paleogeography, subduction, and horizontal underthrusting below Tibet: paradoxes, controvercies, and opportunities. Natl. Sci. Rev. 9 (8) https://doi.org/10.1093/nsr/nwac074.
- van Hinsbergen, D.J.J., Steinberger, B., Doubrovine, P.V., Gassmöller, R., 2011.

 Acceleration and deceleration of India-Asia convergence since the cretaceous: Roles of mantle plumes and continental collision. J. Geophys. Res. Solid Earth 116 (B6).
- Wang, J.-G., Hu, X., Garzanti, E., BouDagher-Fadel, M.K., Liu, Z.-C., Li, J., Wu, F.-Y., 2020. From extension to tectonic inversion: Mid-cretaceous onset of Andean-type orogeny in the Lhasa block and early topographic growth of Tibet: GSA. Bulletin 132 (11–12), 2432–2454.
- Wei, Y., Zhang, K., Garzione, C.N., Xu, Y., Song, B., Ji, J., 2016. Low palaeoelevation of the northern Lhasa terrane during late Eocene: Fossil foraminifera and stable isotope evidence from the Gerze Basin. Sci. Rep. 6 (1), 27508.
- Wu, F.-Y., Ji, W.-Q., Wang, J.-G., Liu, C.-Z., Chung, S.-L., Clift, P.D., 2014. Zircon U-Pb and Hf isotopic constraints on the onset time of India-Asia collision. Am. J. Sci. 314 (2), 548.
- Wu, F., Fang, X., Yang, Y., Dupont-Nivet, G., Nie, J., Fluteau, F., Zhang, T., Han, W., 2022. Reorganization of Asian climate in relation to Tibetan Plateau uplift. Nat. Rev. Earth Environ. 3 (10), 684–700.
- Xiong, Z., Ding, L., Spicer, R.A., Farnsworth, A., Wang, X., Valdes, P.J., Su, T., Zhang, Q., Zhang, L., Cai, F., Wang, H., Li, Z., Song, P., Guo, X., Yue, Y., 2020. The early eocene rise of the Gonjo Basin, SE Tibet: From low desert to high forest. Earth Planet. Sci. Lett. 543, 116312.
- Xiong, Z., Liu, X., Ding, L., Farnsworth, A., Spicer, R.A., Xu, Q., Valdes, P., He, S., Zeng, D., Wang, C., Li, Z., Guo, X., Su, T., Zhao, C., Wang, H., Yue, Y., 2022. The rise and demise of the Paleogene Central Tibetan Valley. Sci. Adv. v. 8 (6) (p. eabj0944).
- Xu, Q., Ding, L., Spicer, R.A., Liu, X., Li, S., Wang, H., 2018. Stable isotopes reveal southward growth of the Himalayan-Tibetan Plateau since the Paleocene. Gondwana Res. 54, 50–61.
- Yakymchuk, C., Holder, R.M., Kendrick, J., Moyen, J.-F., 2023. Europium anomalies in zircon: a signal of crustal depth? Earth Planet. Sci. Lett. 622, 118405.
- Yin, A., Harrison, T.M., 2000. Geologic evolution of the Himalayan-Tibetan orogen. Annu. Rev. Earth Planet. Sci. 28 (1), 211–280.
- Yue, H., Chen, Y.J., Sandvol, E., Ni, J., Hearn, T., Zhou, S., Feng, Y., Ge, Z., Trujillo, A., Wang, Y., Jin, G., Jiang, M., Tang, Y., Liang, X., Wei, S., Wang, H., Fan, W., Liu, Z., 2012. Lithospheric and upper mantle structure of the northeastern Tibetan Plateau. J. Geophys. Res. Solid Earth 117 (B5).
- Zhang, Z., Zhao, G., Santosh, M., Wang, J., Dong, X., Shen, K., 2010. Late cretaceous charnockite with adakitic affinities from the Gangdese batholith, southeastern Tibet: evidence for Neo-Tethyan mid-ocean ridge subduction? Gondwana Res. 17 (4), 615–631.
- Zhang, P., Chen, L., Xiao, W., Zhang, J.E., 2022. Topographic response of Hinterland basins in Tibet to the India–Asia convergence: 3D thermo-mechanical modeling. Front. Earth Sci. 10.
- Zhu, D.-C., Zhao, Z.-D., Niu, Y., Mo, X.-X., Chung, S.-L., Hou, Z.-Q., Wang, L.-Q., Wu, F.-Y., 2011. The Lhasa Terrane: Record of a microcontinent and its histories of drift and growth. Earth Planet. Sci. Lett. 301 (1), 241–255.
- Zhu, D.-C., Wang, Q., Cawood, P.A., Zhao, Z.-D., Mo, X.-X., 2017. Raising the Gangdese Mountains in southern Tibet. J. Geophys. Res. Solid Earth 122 (1), 214–223.
- Zhu, D.-C., Wang, Q., Chung, S.-L., Cawood, P.A., Zhao, Z.-D., 2019. Gangdese Magmatism in Southern Tibet and India–Asia Convergence Since 120 Ma: Geological Society, London, Special Publications, 483, p. 583 no. 1.